Electromagnetic Analysis of an Aperture Modified TEM Cell Including an ITO Layer for Real-Time Observation of Biological Cells Exposed to Microwaves

Malak Soueid[1], Sophie Kohler[1], Lynn Carr[2], Sylvia M. Bardet[2], Rodney P. O'Connor[2], Philippe Leveque[1], and Delia Arnaud-Cormos[1, *]

Abstract—We propose to analyze the aperture and ITO layer presence of a modified transverse electromagnetic (TEM) cell. This TEM cell can be used to study the potential effects of microwave electromagnetic fields on biological cells. This modified delivery device allows real-time observation of biological cells during exposure. Microscopic observation is achieved through an aperture in the lower wall of the TEM cell that is sealed with a 700-nm film of the transparent conducting material Indium tin oxide (ITO). To determine the device efficiency, numerical and experimental electromagnetic dosimetry was conducted. For assessing the effect of the aperture on the specific absorption rate (SAR) in the exposed sample, a plastic Petri dish containing cell culture medium, full-wave 3-D electromagnetic simulations and temperature measurements were performed. For 1-W input power, the SAR values obtained at 1.8 GHz in the sample exposed in the TEM cell with the sealed or non-sealed aperture of 20-mm diameter were 1.1 W/kg and 23.6 W/kg, respectively. An excellent homogeneity of the SAR distribution was achieved when the aperture was sealed with the ITO layer. The performance of the delivery system was confirmed by microwave exposure and simultaneous observation of living cells.

1. INTRODUCTION

Radiofrequency (RF) electromagnetic fields (EMF), from 30 kHz to 300 GHz, are ubiquitous in our daily environment (e.g., in microwave ovens, for mobile telecommunication, Wi-Fi, RADAR). Over the last two decades, the rapid increase in the use of wireless communication devices has been accompanied by a significant amount of research in response to public concern about the possible health effects of RF EMF [1, 2]. However, the mechanisms involved in the interaction between RF EMF and living cells, other than those leading to the acknowledged thermal effects, are still unclear. Real-time visualization of biological cells is important for defining and exploring interaction mechanisms, both for thermal and potential non-thermal effects. However, it is important to define real-time in this context — here we mean real-time from the perspective of biology and not in the microwave (MHz to GHz) regime. Biology and biological responses are transient, far from equilibrium systems that operate on the scale of milliseconds (excitable systems like cardiac and neuronal) to seconds to minutes (cell signals, transcription, protein translation), days to years (development, epigenetics, chronic disease development, etc.). Biological responses are complex and the time scale of measurement must be matched to that of the biological event. For example, if one is trying to observe neural activity in the brain, the sampling frequency must be suited to the transient electrical nature of these events — measuring the mean voltage or end point voltage of the system is not informative. Fluorescent microscopy can be used to study

biological responses that occur over the millisecond to multiple hour timescale. By the application of a wide range of fluorescent probes to cells, one can read out a number of important physiological factors from cells, including changes in ion concentration, pH, voltage and membrane integrity [3].

Most biological studies of RF-EMF thus far have considered arbitrary fixed time points, 30 minute exposure, 4 hr exposure, etc., and therefore are suited only to measuring the integrated endpoints like gene expression, cell death, DNA damage, disease states, animal behaviour, etc. Given that biology is transient, non-equilibrium, and highly adaptive, we propose the development of exposure systems that permit one to study cellular RF-EMF responses with fluorescent microscopy on the scale of biologically relevant events.

As illustrated in [4–6], different exposure systems have been developed to study the health effects of RF EMF. For real-time investigation, specific exposure systems have also been designed incorporating multiple electrode arrays (MEA) [7–9] and coplanar waveguides [10, 11]. A few studies include monitoring of the sample using microscopic imaging. Nevertheless, these systems are typically limited to deliver frequencies higher than 500 MHz. To accommodate the microscope stage for RF applications, existing exposure systems may be adapted by adding an aperture that allows access to the system via a microscope objective. However, such modifications can significantly disturb the electric field induced inside the sample and thus modify the performance of the exposure system.

For *in vitro* studies of RF-induced biological effects at reduced scale, the Transverse Electromagnetic (TEM) cell is a commonly used delivery device [12–16]. An opened TEM cell with an aperture in the center of the lower plate has been proposed for real-time microscopic observation of exposed cells [17]. The diameter of the aperture was comparable to that of the microscope objective. Because of its large size, the impact of the aperture on the electric field distribution inside the exposed sample must be evaluated precisely. In the TEM cell, large samples can be considered like 36-mm Petri dish. This can allow classical biological studies with a large number of cells and with the same exposure setup, i.e., in the same exposure conditions. The control of the temperature is easier compared than in a small volume. For long term exposure, the volume permits to better control the biological environment. The vertical electric field orientation is usually well controlled over a large frequency bandwidth. Due to cell large available surface, many cells can be observed.

In this paper, we propose to seal the aperture with an optically transparent conducting material. We chose a 700-nm layer of Indium tin oxide (ITO) as conducting material, as it is one of the best candidates among the transparent conducting oxides [18]. ITO films have been reported for several purposes, e.g., for manufacturing electrodes for optoelectronic devices [19], electrochromic cells [20], solar cells [21] or for the development of transparent antennas for wireless communication [22–26].

The aim of this study was: (i) to analyze the impact of the aperture versus its diameter and the frequency of the electromagnetic waves (ii) to assess the role of ITO layer on the energy absorbed by a biological sample exposed *in vitro* to EMF at 1.8 GHz. The paper is organized as follows. Section 2 describes the materials and methods for the experiments and numerical modeling. The results and electromagnetic analyses are presented in Section 3 while Section 4 concludes the work.

2. MATERIAL AND METHODS

2.1. Delivery Device

2.1.1. Opened TEM Cell

A TEM cell is an efficient device for *in vitro* studies of EMF-induced effects on living cells. It is known that small TEM cells have a high useful frequency band. We have previously used the TEM cell shown in Figure 1 as a delivery system for microwaves [8, 9, 14, 27, 28] and for nanosecond electric pulses [17, 29, 30]. The biological sample was placed in a 35-mm Petri dish centered above the TEM cell lower plate. The total height of the TEM cell was deliberately set to 20 mm to allow the insertion in the microscope stage. A 12-mm distance between the septum and the lower plate was chosen to allow inserting a Petri dish below the septum of the TEM cell. For this type of TEM cells where the height is rather small compared to the septum width, the E-field has a good uniformity over the TEM cell height [28]. Due to the size of the microscope objective, an aperture with a diameter of 20 mm was made in the center of the lower TEM cell ground plate to allow real-time microscopic observation.
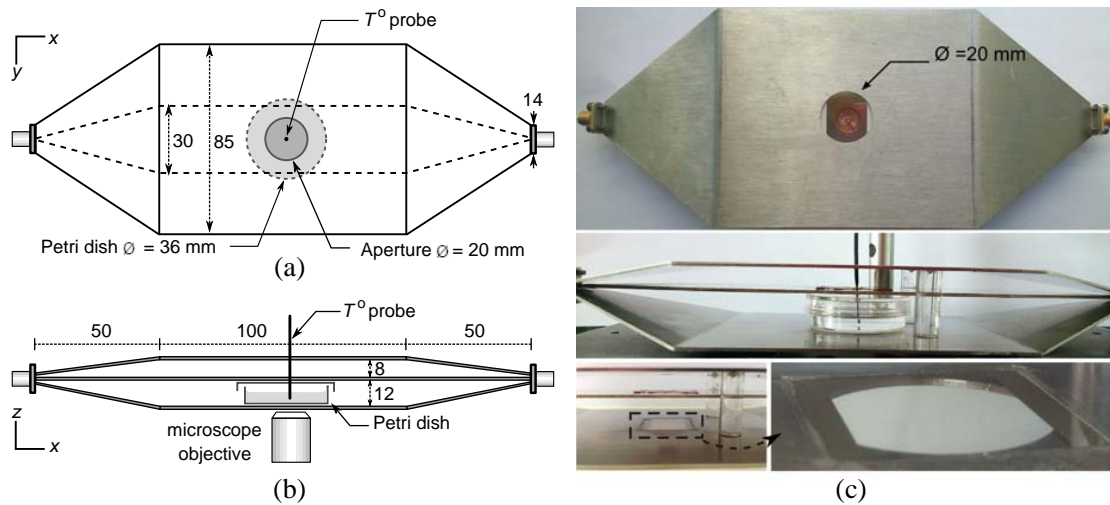
Figure 1. TEM cell containing the Petri dish. (a) Bottom view. (b) Side view. (c) Photos of the TEM and ITO film placed in the bottom plate of the TEM Cell (Bottom view, side view and aperture with ITO film). Dimensions are in mm.

2.1.2. ITO Characteristics

The ITO material used to cover the TEM cell lower aperture is a mixture of indium(III) oxide (In_2O_3) and tin(IV) oxide (SnO_2) [31]. In powder form, ITO is yellow-green in color. When deposited on glass or clear plastic as a thin film of maximum 1-µm thickness, it is transparent, colorless, and functions as an electrical conductor. For good electrical conductive properties of the ITO layer at microwave frequencies, the material thickness should be adequate. Typically, thicknesses of a few hundred nm, corresponding to an acceptable skin depth/ITO layer thickness ratio (2%), are used [32]. It has been shown in the literature that an optical transparency of 90% was reached for an ITO film thickness around 370-nm [32]. This transparency decreases to 70% when the thickness increases to 1100-nm. With an optical transparency lower than 70% microscopic observation of biological cells becomes more difficult. A thickness of 700 nm was chosen to ensure a good conductive behavior. With this ITO layer thickness, an optical transparency of 85% was achieved. So, a 700-nm ITO layer deposited on a 22-mm^2 glass plate with 170-µm thickness (Brand Indium-Tin-Oxide Coated cover slips, 06473B-AB, SPI Supplies, USA) was selected to respect the working distance of the microscope objective.

2.1.3. Studied Configurations

To study the influence of the aperture and the ITO layer on the device performance, different configurations of the TEM cell containing a Petri dish filled with a 3-ml buffered salt solution, were studied:

- A configuration without aperture.
- Several configurations where the diameter of the aperture was varied from 2 mm up to 20 mm.
- A configuration where the 20-mm diameter aperture was sealed with a 700-nm ITO layer.

2.2. Experimental Measurements

The exposure system was experimentally characterized by measuring two significant parameters: the S-parameters and the distribution of the Specific Absorption Rate (SAR) in the biological sample.
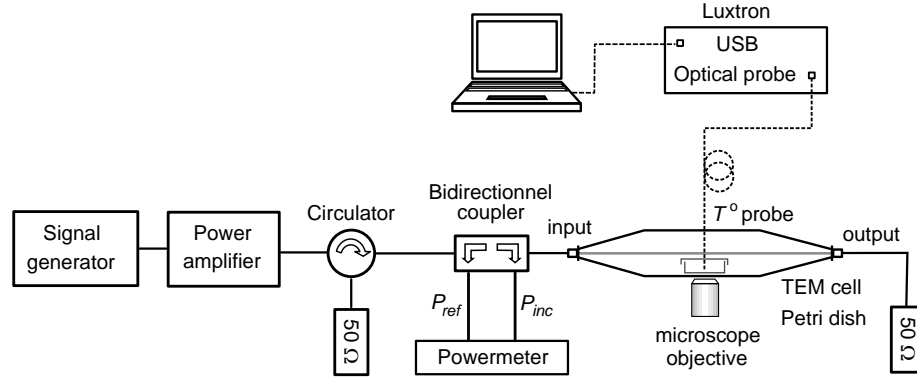
Figure 2. Experimental setup developed for temperature measurements (using the Luxtron probe).

2.2.1. S_{ij} Measurements

To characterize the frequency bandwidth of the delivery system, reflection and transmission coefficients were measured up to 3 GHz. Different configurations were measured: the TEM cell with an aperture of varying diameter with or without ITO layer, and containing an empty Petri dish or a Petri dish filled with 3-ml of buffered salt solution. The S_{ij} parameters were obtained by connecting the TEM cell to a vector network analyzer (HP 8753E, Agilent) presenting a 50-Ω input impedance.

2.2.2. SAR Assessment

To achieve high quality biological investigations as indicated in [33], SAR distribution was experimentally and numerically evaluated at 1.8 GHz. The SAR was evaluated through 3D simulations and temperature measurements. The experimental setup for SAR measurements is shown in Figure 2. Continuous-wave (CW) RF signals were delivered by a signal generator (HP8648B, Hewlett-Packard, USA) connected to a power amplifier (M.19.40.50. 850-1950.44.25, Nuclétudes, France) with a 40-dB gain. A high power 50-Ω load connected to the TEM cell output port ensured impedance matching. A bidirectional coupler allowed monitoring of the incident and reflected powers at the input of the TEM cell.

The temperature measurements were performed using a non-perturbing fluoroptic probe (Luxtron One, Lumasense Technologies, CA, USA). The temperature measurements were recorded at a rate of 4 samples per second. The probe tip was vertically immersed in the Petri dish. Measurements were conducted at different positions along the x and y axis. Before RF EMF exposure, a 30-min time delay was required to guarantee temperature stability. The SAR was computed using Equation (1),

$$\text{SAR} = C \left. \frac{\partial T}{\partial t} \right|_{t=0} \quad \text{(W/kg)} \tag{1}$$

where C is the specific heat capacity of the considered medium, 4186 J/(kg·K) and $\partial T/\partial t$ corresponds to the initial slope of the rate of temperature increase versus time.

2.3. Electromagnetic Analysis

To complete the experimental measurements, full-wave 3-D simulations were performed using commercial software (CST Microwave Studio). The code implements the Finite Integration Technique (FIT), based on a discretization of Maxwell's equations in integral form. It allows dosimetric computations directly in the form of average SAR or maximum SAR over the exposed sample. From the electric field, the spatial distribution of the SAR (W/kg) can be deduced using:

$$\text{SAR} = \frac{\sigma E^2}{2\rho} \quad \text{(W/kg)} \tag{2}$$

where E is the amplitude of the electric field (V/m), ρ is the mass density (kg/m^3) and σ is the electrical conductivity (S/m) of the exposed sample. Average SAR is obtained by dividing the total power absorbed in the biological sample by the full sample mass, while maximum SAR is given as a numerical value per volume element without mass or volume averaging and becomes a space distribution function. This function, called local SAR, ensure SAR distribution that's can not be determined by measurement.

The structure was simulated and the results were extracted over the 0.5–3 GHz frequency band for an incident power of 1 W. The feeding source and the load are modeled by waveguide ports having 50-Ω impedance. The Petri dish cover glass permittivity was set to 2.5. The dielectric properties of the solution at 1.8 GHz were: conductivity of 2.5 S/m, relative permittivity of 76 and mass density of 1000 kg/m^3. The metallic parts were considered perfect electric conductors. The ITO layer had a conductivity of 1.3×10^6 S/m as deposited on a glass plate with a relative permittivity of 4.8 [31]. The TEM cell's long axis is oriented along the Ox axis, being centered in the origin of the coordinate system. The height of the cell is on the Oz axis. The mesh is produced by an automatic mesh generator, which ensures a good compromise between accuracy and simulation time. Due to the various dimensions of the simulated structure and for more precision, the biological sample was meshed with a uniform grid mesh of 250 μm. When the ITO layer was included, a non-uniform mesh with a finest grid Δz resolution of 0.35 μm was used.

2.4. Biological Sample Preparation and Fluorescence Microscopy

The U87MG human glioblastoma cell line (a type of brain cancer cell), was used in these experiments. Cells were grown in complete culture medium (MEM supplemented with 10% fetal bovine serum, glutamine, 100 units/ml penicillin and 100 μg/ml streptomycin; Invitrogen) in an incubator at 37°C and with 5% CO$_2$. Cells were subcultured onto glass-bottom, poly-D-lysine coated Petri dishes (Fluodish; WPI-Europe) at a density of 1–2 $\times$ 10^5 cells per ml and allowed to adhere and grow for 48 hours prior to experiments. Cells were transfected with CellLight$^®$ tubulin-GFP vector (Invitrogen) 18 hours prior to experiments and then loaded with tetramethylrhodamine methyl ester (TMRM; Invitrogen) and Hoechst-33342 (Invitrogen), to visualize microtubules, mitochondria and nuclei, respectively. These fluorescent dyes were chosen as examples that can be used to report both structural and functional changes in living cells. Culture media and dyes were removed and replaced with 3 ml of HEPES buffered salt solution (Live cell Imaging Solution; Invitrogen), in order to maintain physiological conditions with respect to osmolarity, pH and membrane potential.

Epifluorescent illumination of the cells was accomplished with a solid state light engine (Spectra 7, Lumencor), coupled to the microscope (DMI6000, Leica) by a 1-mm quartz fiber. Light in the ultraviolet (390/18), cyan (475/28) and green (549/15) channels was used to excite Hoechst-33342, GFP and TMRM, respectively. Emitted light was separated from excitation with a dichroic beamsplitter (89100BS, Chroma) and selected by emission filters controlled by a filter wheel (MAC 6000, Ludl). Images were captured on an electron multiplying charge coupled device camera (EMCCD Evolve 512, Roper) with 512 $\times$ 512 pixels. Cells were illuminated for short durations (50 ms) to minimize photobleaching. Images were background corrected with a region of interest not containing cells.

3. RESULTS

3.1. S-Parameter

The results of the measurements and simulations show that the presence of the culture medium and the different aperture sizes slightly modifies the transmission and reflection parameters of the TEM cell. The measurements presented in Figure 3 correspond to three different configurations: the TEM cell without aperture, with the 20-mm diameter aperture and with the 20-mm diameter aperture sealed by the 700-nm ITO layer. For the three configurations, the return loss shows good impedance matching up to 2.2 GHz and the transmission coefficient is comprised between 0 and -1 dB up to 3 GHz. For the designed structure, the higher order mode cutoff frequencies have been assessed. The first order cutoff frequency can be extrapolated from the results proposed by [34, 35]. Considering the ratio between the

30-mm strip width and the 21-mm height, a cutoff frequency around 6 GHz is obtained. This value corresponds to a symmetrical structure but it is high enough to support the TEM-cell use up to 3 GHz.

The periodic resonances observed are due to the transitions between the connectors and the TEM cell. Indeed, the minimums and maximums can be associated to the strip line length and are due to the small mismatch between TEM cell plates and the coaxial connectors. By considering the 22-cm TEM cell length including connectors, the frequency of the equivalent half wavelength dipole is around 650 MHz. This frequency value and its harmonics are consistent with the S-parameters minimums and maximums on the Figure 3. This mismatch remains low with proper S-parameters. However, to reduce the reflection coefficient, the design of the TEM cell particularly in the connectors' area has to be improved for exposures at frequencies higher than 2.4 GHz.

3.2. Experimental Dosimetry

Results of three different configurations, corresponding to the TEM cell without aperture and with a 20-mm diameter aperture are presented in Figure 4. In the later case, the ITO layer was present or not in the aperture. The incident power was set to 25 W. Temperature data are plotted in Figure 3. The RF generator was switched on after 20 min of acquisition (only 1 min is plotted). We have made more than 20 measurements for each of the three different configurations. The computation of the standard deviation takes also into account the uncertainty of the SAR assessment. We used an exponential fit of the temperature measurements to compute the exponential fit derivative at the initial phase ($t = 0$ s, RF on). The derivative slightly varies depending on the chosen parameters, specifically on the time window for the fit computation. In our case, we have varied the time window from 30 s to 120 s. For each measurement and for each different time windows, a SAR value was assessed. The standard deviation was calculated from all the assessed SAR values, i.e., 60 SAR values (20 measurements with 3 time windows). This allowed defining a standard deviation on the measurements. The exponential fit was obtained using an unconstrained nonlinear optimization (derivative-free method, fminsearch matlab® optimization function).

The associated SAR values and standard deviation calculated from temperature are summarized in Table 1 (measurements). In our conditions, as the SAR is a linear quantity with respect to the input power, it is convenient to express the SAR normalized per unit of input power (W/kg/W). A good agreement was observed between the SAR values measured in the TEM cell without the aperture and with the aperture closed by the 700-nm ITO layer. These normalized SAR values show excellent agreement with numerical simulations, which confirms the electrical continuity in the TEM cell aperture
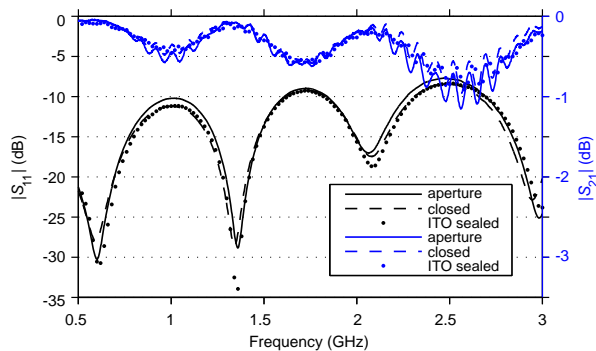

Figure 3. S_{11} (black line) and S_{21} (blue line) parameters of the TEM cell without aperture (closed), with the 20-mm diameter aperture (aperture) and with the 20-mm diameter aperture sealed by the 700-nm ITO layer (ITO sealed aperture).
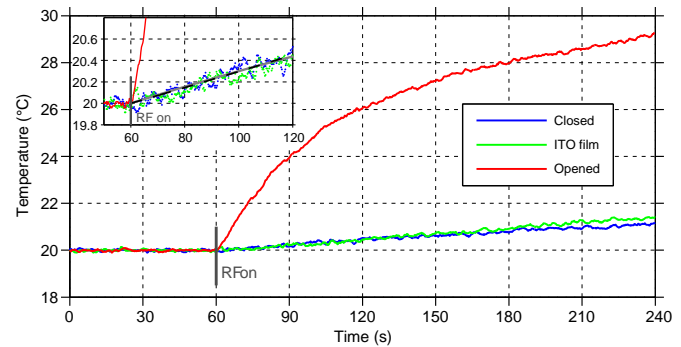
Figure 4. Temperature measurements recorded by the Luxtron probe obtained for three different configurations: closed TEM cell (blue curve); lower aperture sealed by 700 nm ITO film (green curve); TEM cell with 20 mm diameter lower aperture (red curve). In the inset, the exponential temperature fit obtained using an unconstrained nonlinear optimization is presented.

closed by the ITO layer. For the TEM cell with the 20-mm diameter aperture, a significant increase in the local SAR value (23.6 ± 0.6 W/kg/W) was observed compared to the two other configurations. This indicates that the presence of the circular aperture highly affects the local SAR in the center of the biological solution. To better understand the influence of the aperture, a parametric study using 3D electromagnetic simulations was carried out as a function of the aperture size and frequency.

3.3. Electromagnetic Analysis

Dosimetric computations were performed to obtain the SAR averaged over the whole volume of the exposed sample along with the local SAR averaged in $1 \, \mathrm{mm}^3$ cubes at the bottom center of the Petri dish. This local SAR corresponds to the probe measurement volume.

As indicated in Table 1, a good level of consistency was obtained between the numerical and the experimental SAR values. The knowledge of the SAR distribution is essential in microdosimetric investigations of biochemical effects at the level of cellular dimension and below. Figure 5 shows the SAR distribution across the bottom layer and a vertical cut (xOz plane) across the middle of the biological sample at 1.8 GHz. Three configurations are presented: the TEM cell without aperture, with a 20 mm diameter lower aperture and with the lower aperture sealed by 700-nm ITO layer. High SAR levels are observed above the aperture (Figure 5(b)). The aperture significantly modifies the SAR distribution with an increased heterogeneity. Thus, it is recommended to close the aperture with an ITO layer to prevent leakage and maintain good homogeneity in the biological solution.

To further understand the influence of the aperture size on the SAR distribution within the biological medium, different configurations with an aperture diameter varying from 0 to 20 mm with a step of 2 mm were simulated. Figure 6 presents the local SAR variation at 1.8 GHz for different aperture sizes. As observed, the bottom layer SAR value increases with the aperture size. This confirms the high influence of the aperture size on the local SAR value.

As seen in Figure 6, for aperture diameters smaller then 8 mm the SAR inhomogeneity is acceptable

Table 1. Localized measured and simulated SAR for 3 configurations at 1.8 GHz.

TEM Cell	SAR (W/kg/W$_{\mathrm{inc}}$)	
	Measurements*	Simulation
Without aperture	1.17 ± 0.14	1.10
With 20-mm aperture sealed with ITO	1.10 ± 0.13	1.05
With 20-mm diameter aperture	23.6 ± 0.6	21.8

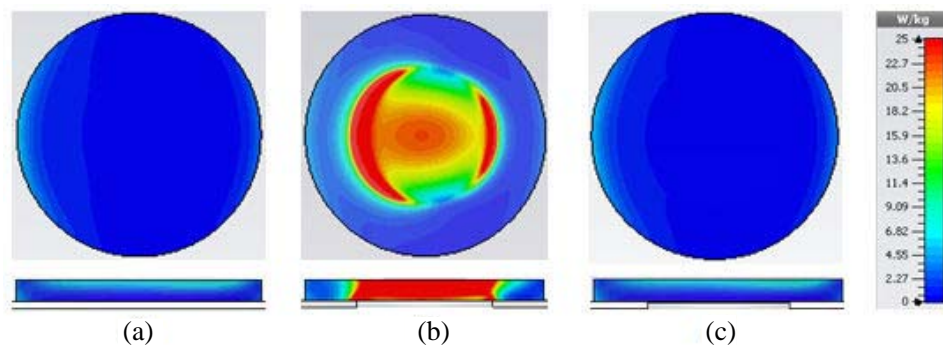*Measurements incident power = 25 W.

(a) (b) (c)

Figure 5. SAR distribution across the bottom layer and a vertical cut of the biological sample for three different configurations: (a) TEM cell without aperture, (b) TEM cell with 20 mm diameter lower aperture, (c) 20-mm diameter lower aperture sealed by 700 nm ITO layer.
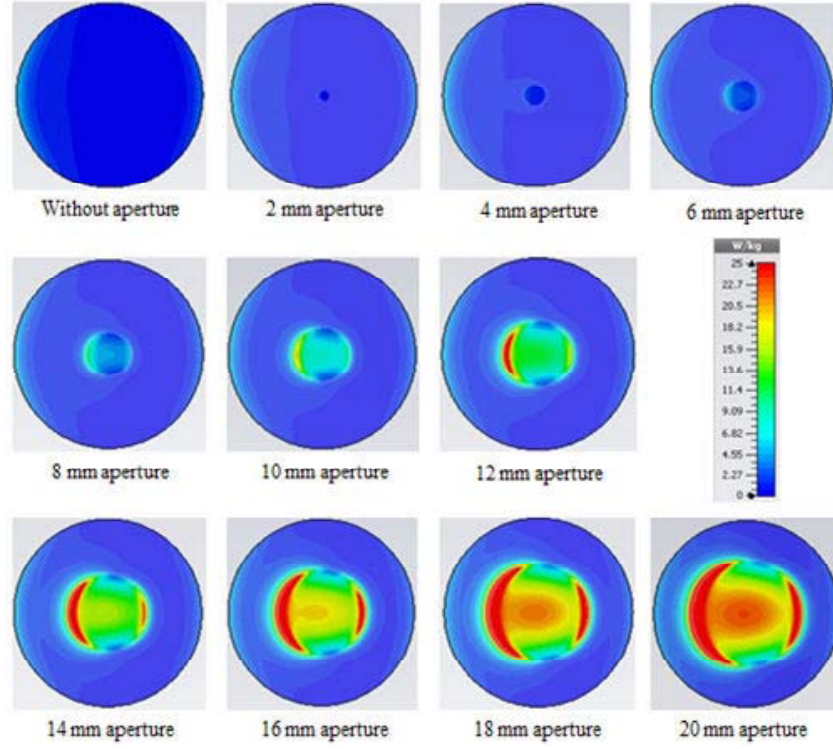
Figure 6. SAR distribution at 1.8 GHz across the bottom layer of the biological sample obtained for different size of aperture drilled in the lower TEM cell plate without ITO layer.

indicating that the electric field focusing on the aperture edge is weak. On the contrary, when increasing the aperture dimension (a diameter higher than 8 mm), the SAR variability increases indicating that the electric field focusing on the aperture edge is enhanced, thereby inducing higher SAR inhomogeneity in the region above the aperture.

In addition, the SAR averaged over the whole volume depending on the frequency and for different aperture sizes (diameter varying from 0 to 20 mm with a step of 4 mm) was calculated and shown in Figure 7. For all simulated cases, the SAR value increases with the aperture size and frequency up to 2 GHz. Above 2 GHz, resonances appear at certain frequencies for all configurations. These frequencies can be related to the mode of the equivalent cylindrical dielectric resonator representing the solution in the Petri dish. A significant variation of the SAR is observed. This variation differs from one configuration to another, which confirms the high impact of the aperture size on the SAR value due to the induced leakage. To support the resonance frequencies, some measurements have been made (data not shown). These measurements have highlighted similar changes of the SAR values versus the frequency with maximums close to those obtain by simulation for the whole volume.

For the TEM cell without aperture, the computed SAR resonance occurred at 2.7 GHz. An analytical approximation of the structure was evaluated to identify this resonance frequency. The biological sample placed in the Petri dish is assimilated to a cylindrical dielectric resonator with the lower TEM cell metallic plate as an electric short circuit. The continuity conditions at the other interfaces of the sample can be approach to magnetic short circuit due to the passage from a high relative dielectric permittivity, $\varepsilon_{r1} = 76$ the liquid sample, to a low relative dielectric permittivity ($\varepsilon_{r2} = 2.5$ for the Petri dish and $\varepsilon_{r3} = 1$ for the vacuum). The resonant frequencies are given by:

$$f_{\mathrm{RTE}_{nm}} = \frac{c}{2\pi\sqrt{\varepsilon_r\mu_r}}\sqrt{\left(\frac{\chi_{nm}}{a}\right)^2 + \left(\frac{\pi}{2h}\right)^2} \tag{3}$$

where $h = 3.1$ mm and $a = 17.5$ mm represent the height and radius, respectively, of the liquid sample; χ_{nm} corresponds to the nth zero of the Bessel function of order n; $c = 3.10^8$ m/s is the speed of light
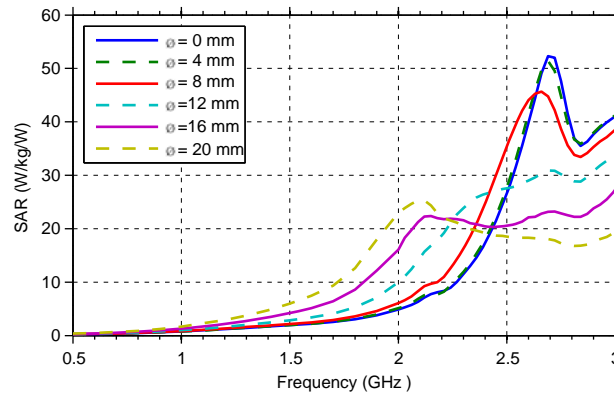
Figure 7. SAR averaged over the whole volume depending on the frequency for different aperture sizes (a diameter of 0, 4, 8, 12, 16 and 20 mm).
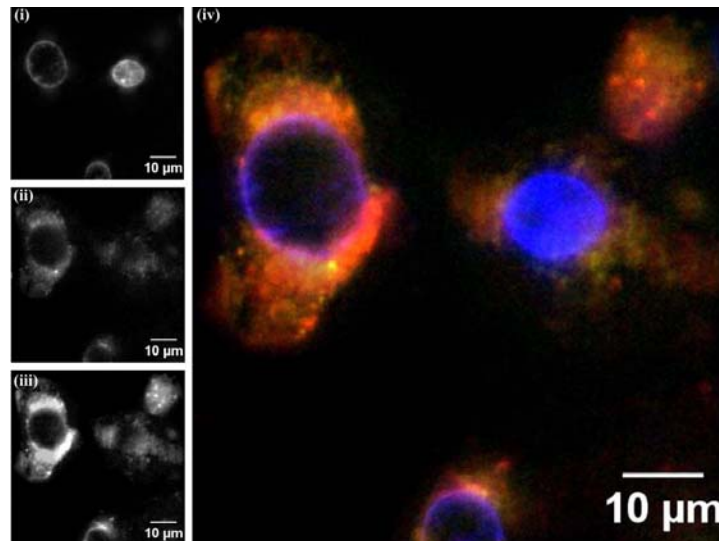

Figure 8. Multicolour fluorescent images of U87 cells acquired through the ITO-aperture TEM cell. Cells were loaded with fluorophores to label i, nuclei (Hoechst-33342), ii, microtubules with tubulin-GFP and iii, mitochondria (TMRM), iv, a composite image overlaying all three fluorescent channels. Images were acquired with a Leica HCX 40x long working distance objective (N.A. 0.75).

and $\varepsilon_r = 76$ the relative permittivity of the liquid sample. For the TEM cell without aperture, the computed SAR resonance occurred at 2.7 GHz. The first theoretical resonance frequency (TE_{01} mode) is 2.85 GHz. The resonant frequencies obtained by analytical approximation and by simulation are in good agreement.

3.4. Cellular Imaging with Live-Cell Fluorescence Microscopy

Live-cell fluorescent images were acquired with high resolution through the ITO-coated window aperture with the glass-bottom Petri dish located in the TEM cell. Cells were labeled using three commonly used fluorophores (Hoechst, green fluorescent protein (GFP) and TMRM) to demonstrate the potential of this setup for live-cell imaging experiments. The addition of the thin ITO glass layer with the glass cover slide of the Petri dish increases the optical path and therefore imposes a limitation on the choice of objective. Nevertheless, the use of long-working distance objectives obviates this limitation, allowing the visualization of sub-cellular compartments and organelles with high resolution (Figure 8).

4. CONCLUSION

In this paper, a modified TEM cell was proposed for the real time observation of biological cells exposed to microwaves. A 20-mm diameter aperture was drilled in the lower plate of the TEM cell and sealed with a 700-nm thick ITO layer, a specific material with both electrical conductivity and optical transparency. Electromagnetic analysis was conducted in a Petri dish placed within the TEM cell. Results showed a good level of consistency between the SAR values evaluated via temperature measurements and numerical results. The TEM cell without aperture and with aperture sealed with the 700-nm ITO layer presented the same SAR values and a good homogeneity in SAR distribution. In summary, we demonstrated that the ITO layer is a good solution to avoid perturbation of the SAR distribution by the aperture, allowing the possibility of real time observation during EM exposure of living cells. Our exposure system will facilitate future experiments examining the potential transient events that occur on the scale of cellular imaging experiments (over milliseconds, seconds, minutes and hours).

ACKNOWLEDGMENT

REFERENCES

1. Lin, J. C., "Studies on microwaves in medicine and biology: From snails to humans," *Bioelectromagnetics*, Vol. 25, 146–159, 2004.
2. Valberg, P. A., T. E. van Deventer, and M. H. Repacholi, "Workgroup report: Base stations and wireless networks-radiofrequency (RF) exposures and health consequences," *Environmental Health Perspectives*, Vol. 115, 416–424, Mar. 2007.
3. Mason, W. T., *Fluorescent and Luminescent Probes for Biological Activity: A Practical Guide to Technology for Quantitative Real-time Analysis*, 2nd Edition, Academic Press, New York, 1999.
4. Paffi, A., F. Apollonio, G. A. Lovisolo, C. Marino, R. Pinto, M. Repacholi, et al., "Considerations for developing an RF exposure system: A review for in vitro biological experiments," *IEEE Transactions on Microwave Theory and Techniques*, Vol. 58, 2702–2714, Oct. 2010.
5. Paffi, A., C. Merla, R. Pinto, G. A. Lovisolo, M. Liberti, C. Marino, et al., "Microwave exposure systems for in vivo biological experiments: A systematic review," *IEEE Transactions on Microwave Theory and Techniques*, Vol. 61, 1980–1993, 2013.
6. Balzano, Q., C. K. Chou, R. Cicchetti, A. Faraone, and R. Y. S. Tay, "An efficient RF exposure system with precise whole-body average SAR determination for in vivo animal studies at 900 MHz," *IEEE Transactions on Microwave Theory and Techniques*, Vol. 48, 2040–2049, 2000.
7. Koester, P., J. Sakowski, W. Baumann, H.-W. Glock, and J. Gimsa, "A new exposure system for the in vitro detection of GHz field effects on neuronal networks," *Bioelectrochemistry*, Vol. 70, 104–114, 2007.
8. Merla, C., N. Ticaud, D. Arnaud-Cormos, B. Veyret, and P. Leveque, "Real-time RF exposure setup based on a multiple electrode array (MEA) for electrophysiological recording of neuronal networks," *IEEE Transactions on Microwave Theory and Techniques*, Vol. 59, 755–762, Mar. 2011.
9. Moretti, D., A. Garenne, E. Haro, F. Poulletier de Gannes, I. Lagroye, P. Leveque, et al., "In-vitro exposure of neuronal networks to the GSM-1800 signal," *Bioelectromagnetics*, Vol. 34, 571–578, Dec. 2013.
10. Liberti, M., F. Apollonio, A. Paffi, M. Pellegrino, and G. D'Inzeo, "A coplanar-waveguide system for cells exposure during electrophysiological recordings," *IEEE Transactions on Microwave Theory and Techniques*, Vol. 52, 2521–2528, 2004.
11. Paffi, A., M. Pellegrino, R. Beccherelli, F. Apollonio, M. Liberti, D. Platano, et al., "A real-time exposure system for electrophysiological recording in brain slices," *IEEE Transactions on Microwave Theory and Techniques*, Vol. 55, 2463–2471, 2007.

12. Paffi, A., M. Liberti, F. Fratta, F. Apollonio, C. Merla, R. Pinto, et al., "A TEM cell system for in vivo exposure at 2.45 GHz," *2012 6th European Conference on Antennas and Propagation (EUCAP)*, 1099–1101, 2012.

13. Crawford, M. L., "Generation of standard EM fields using TEM transmission cells," *IEEE Transactions on Electromagnetic Compatibility*, Vol. 16, 189–195, 1974.

14. O'Connor, R. P., S. D. Madison, P. Leveque, H. L. Roderick, and M. D. Bootman, "Exposure to GSM RF fields does not affect calcium homeostasis in human endothelial cells, rat pheocromocytoma cells or rat hippocampal neurons," *Plos One*, Vol. 5, 16, Jul. 2010.

15. Zhao, J. X., H. M. Lu, and J. Deng, "Dosimetry and temperature evaluations of a 1800 MHz TEM cell for in vitro exposure with standing waves," *Progress In Electromagnetics Research*, Vol. 124, 487–510, 2012.

16. Iftode, C. and S. Miclaus, "Design and validation of a TEM cell used for radiofrequency dosimetric studies," *Progress In Electromagnetics Research*, Vol. 132, 369–388, 2012.

17. Kohler, S., R. P. O'Connor, V. Thi Dan Thao, P. Leveque, and D. Arnaud-Cormos, "Experimental microdosimetry techniques for biological cells exposed to nanosecond pulsed electric fields using microfluorimetry," *IEEE Transactions on Microwave Theory and Techniques*, Vol. 61, 2015–2022, 2013.

18. Yasin, T., R. Baktur, and C. Furse, "A comparative study on two types of transparent patch antennas," *2011 XXXth URSI General Assembly and Scientific Symposium*, 1–4, 2011.

19. Sato, H., H. Fujikake, T. Murashige, H. Kikuchi, T. Kurita, and F. Sato, "A4-sized flexible ferroelectric liquid-crystal displays with micro color filters," *Journal of the Society for Information Display*, Vol. 13, 461–468, Jun. 2005.

20. Beaupre, S., J. Dumas, and M. Leclerc, "Toward the development of new textile/plastic electrochromic cells using triphenylamine-based copolymers," *Chemistry of Materials*, Vol. 18, 4011–4018, Aug. 2006.

21. Zhao, L., Z. B. Zhou, H. Peng, and R. Q. Cui, "Indium tin oxide thin films by bias magnetron RF sputtering for heterojunction solar cells application," *Applied Surface Science*, Vol. 252, 385–392, Oct. 2005.

22. Bourry, M., M. Sarret, and M. Drissi, "Novel ITO alloy for microwave and optical applications," *48th Midwest Symposium on Circuits and Systems*, Vol. 1, 615–618, 2005.

23. Lee, C.-T., C.-M. Lee, and C.-H. Luo, "The transparent monopole antenna for WCDMA and WLAN," *IEEE Annual Wireless and Microwave Technology Conference, WAMICON' 06*, 1–3, 2006.

24. Pakorn, P., S. Porntheeraphat, A. Klamchuen, and J. Nukeaw, "ITO thin films prepared by gas-timing RF magnetron sputtering for transparent flexible antenna," *2nd IEEE International Conference on Nano/Micro Engineered and Molecular Systems, NEMS' 07*, 647–650, 2007.

25. Colombel, F., X. Castel, M. Himdi, G. Legeay, S. Vigneron, and E. M. Cruz, "Ultrathin metal layer, ITO film and ITO/Cu/ITO multilayer towards transparent antenna," *IET Science Measurement & Technology*, Vol. 3, 229–234, May 2009.

26. Neveu, N., M. Garcia, J. Casana, R. Dettloff, D. R. Jackson, and C. Ji, "Transparent microstrip antennas for CubeSat applications," *2013 IEEE International Conference on Wireless for Space and Extreme Environments (WiSEE)*, 1–4, 2013.

27. Moisescu, M. G., P. Leveque, J.-R. Bertrand, E. Kovacs, and L. M. Mir, "Microscopic observation of living cells during their exposure to modulated electromagnetic fields," *19th Biannual International Symposium on Bioelectrochemistry and Bioenergetics*, 9–15, Toulouse, France, 2007.

28. Kohler, S., N. Ticaud, M.-M. Iordache, M. G. Moisescu, T. Savopol, P. Leveque, and D. Arnaud-Cormos, "Setup for simultaneous microwave heating and real-time spectrofluorometric measurements in biological systems," *Progress In Electromagnetics Research*, Vol. 145, 229–240, 2014.

29. Kohler, S., P. Jarrige, N. Ticaud, R. P. O'Connor, L. Duvillaret, G. Gaborit, et al., "Simultaneous high intensity ultrashort pulsed electric field and temperature measurements using a unique electro-optic probe," *IEEE Microwave and Wireless Components Letters*, Vol. 22, 153–155, 2012.

30. Kohler, S., T. D. T. Vu, P. T. Vernier, P. Leveque, and D. Arnaud-Cormos, "Characterization of a TEM cell-based setup for the exposure of biological cell suspensions to high-intensity nanosecond pulsed electric fields (nsPEFs)," *2012 IEEE MTT-S International Microwave Symposium Digest (MTT)*, 1–3, Montréal, Canada, 2012.

31. Granqvist, C. G. and A. Hultaker, "Transparent and conducting ITO films: New developments and applications," *Thin Solid Films*, Vol. 411, 1–5, May 2002.

32. Yasin, T., R. Baktur, and C. Furse, "A study on the efficiency of transparent patch antennas designed from conductive oxide films," *2011 IEEE International Symposium on Antennas and Propagation (APSURSI)*, 3078–3080, 2011.

33. Kuster, N. and F. Schönborn, "Recommended minimal requirements and development guidelines for exposure setups of bio-experiments addressing the health risk concern of wireless communications," *Bioelectromagnetics*, Vol. 21, 508–514, 2000.

34. Yang, H. and S. Lee, "A variational calculation for higher order mode cutoff frequencies of a symmetrical strip line by conformal mapping," *Microwave and Optical Technology Letters*, Vol. 32, 449–452, Mar. 2002.

35. Tsitsos, S., A. A. P. Gibson, and A. H. I. McCormick, "Higher-order modes in coupled striplines — Prediction and measurement," *IEEE Transactions on Microwave Theory and Techniques*, Vol. 42, 2071–2077, Nov. 1994.